Evaluation of the bioactivity of fluoride-enriched mineral trioxide aggregate on osteoblasts

Proksch, S ; Brossart, J ; Vach, K ; Hellwig, E ; Altenburger, M J ; Karygianni, L

Abstract: AIM To investigate whether a combination of mineral trioxide aggregate (MTA) and fluoride compounds affects bone cells. METHODOLOGY Mineral trioxide aggregate (MTA) discs (ProRoot , Dentsply Sirona, Ballaigues, Switzerland) with and without the addition of 0.1%, 0.25% and 0.5% sodium fluoride were characterized for their surface roughness by laser scanning microscopy and for the adhesion of human alveolar osteoblasts by scanning electron microscopy. Using eluates from fluoride-enriched MTA discs, the cell proliferation was measured by monitoring the DNA incorporation of 5-bromo-2'-deoxyuridine. Further, gene expression was evaluated by qPCR arrays, extracellular matrix mineralization was quantified by absorption measurement of Alizarin red stains, and effects were calculated with repeated measures analysis and post hoc P-value adjustment. RESULTS Irrespective of fluoride addition, cell adhesion was similar on MTA discs, of which the surface roughness was comparable. Control osteoblasts had a curvilinear proliferation pattern peaking at d5, which was levelled out by incubation with MTA. The addition of fluoride partly restored the MTA-related reduction in the cellular proliferation rate in a dose-dependent manner. At the mRNA level, both fluoride and MTA modulated a number of genes involved in osteogenesis, bone mineral metabolism and extracellular matrix formation. Although MTA significantly impaired extracellular matrix mineralization, the addition of fluoride supported the formation of mineralized nodules in a dose-dependent manner. CONCLUSION The addition of fluoride modulated the biocompatibility of MTA in terms of supporting bone cell proliferation and hard tissue formation. Hence, fluoride enrichment is a trend-setting advancement for MTA-based endodontic therapies.

DOI: https://doi.org/10.1111/iej.12905

Evaluation of the Bioactivity of Fluoride-Enriched Mineral Trioxide Aggregate On Osteoblasts

Proksch S[1,2,*], Brossart J[2], Vach K[3], Hellwig E[1,2], Altenburger MJ[2], Karygianni L[2,§]

[1] G.E.R.N. Tissue Replacement, Regeneration & Neogenesis, Department of Operative Dentistry and Periodontology, Medical Center - University of Freiburg, Faculty of Medicine, Albert-Ludwigs-University of Freiburg, Germany, [2] Centre for Dental Medicine, Department of Operative Dentistry and Periodontology, Medical Center - University of Freiburg, Faculty of Medicine, Albert-Ludwigs-University of Freiburg, Germany, [3] Institute of Medical Biometry and Statistics, Medical Center - University of Freiburg, Faculty of Medicine, Albert-Ludwigs-University of Freiburg, Germany, § Present address: Clinic for Preventive Dentistry, Periodontology and Cariology, Center of Dental Medicine, University of Zurich, Switzerland

Key Words Mineral trioxide aggregate (MeSH ID: C086631); Fluoride (MeSH ID: D005459); Osteoblasts (MeSH ID: 010006); Gene Expression (MeSH ID: D015870); Endodontics (MeSH ID: D004708)

Running Title Fluoride-enriched MTA supports osteoblasts

Corresponding Author

PD Dr. Susanne Proksch

G.E.R.N. Tissue Replacement, Regeneration & Neogenesis, Dpt. of Operative Dentistry and Periodontology, Medical Center - University of Freiburg, Faculty of Medicine, Albert-Ludwigs-University of Freiburg, Engesserstr. 4, 79108 Freiburg, Germany

Email: susanne.proksch@uniklinik-freiburg.de

Phone: 0049-761-270 49311

Fax: 0049-761-270 47390

ABSTRACT

Aim Since both mineral trioxide aggregate (MTA) and fluoride are widely recognized for their hard tissue-inductive properties, the present study aimed to investigate if a combination of both compounds affects bone cells.

Methodology MTA disks (ProRoot®, Dentsply, Germany) with and without addition of 0.1%, 0.25%, and 0.5% sodium fluoride were characterized for their surface roughness by laser scanning microscopy and for the adhesion of human alveolar osteoblasts by scanning electron microscopy. Using eluates from fluoride-enriched MTA disks, the cell proliferation was measured by monitoring the DNA incorporation of 5-bromo-2'-deoxyuridine. Further, gene expression was evaluated by qPCR arrays, extracellular matrix mineralization was quantified by absorption measurement of Alizarin red stains, and effects were calculated with repeated measures analysis and post hoc *p*-value adjustment.

Results Irrespective of fluoride addition, cell adhesion was similar on MTA disks, of which the surface roughness was comparable. Control osteoblasts had a curvilinear proliferation pattern peaking at d5, which was leveled out by incubation with MTA. The addition of fluoride partly restored the MTA-related reduction of the cellular proliferation rate in a dose-dependent manner. At the mRNA level, both fluoride and MTA modulated a number of genes involved in osteogenesis, bone mineral metabolism and extracellular matrix formation.

Although MTA significantly impaired extracellular matrix mineralization, the addition of fluoride supported the formation of mineralized nodules in a dose-dependent manner.

Conclusion The addition of fluoride modulated the biocompatibility of MTA in terms of supporting bone cell proliferation and hard tissue formation. Hence, fluoride enrichment is a trend-setting advancement for MTA-based endodontic therapies.

Introduction

Mineral trioxide aggregrate (MTA) fulfills the prerequisites of an endodontic repair material, i.e. adhering to tooth hard tissues and providing sufficient seal while being stable, radiopaque and biocompatible (Roberts *et al.* 2008). The major components of hygroscopic MTA are tricalcium silicate, tricalcium aluminate, calcium silicate and tetracalcium aluminoferrite (Lee *et al.* 2004, Nekoofar *et al.* 2011, Grazziotin-Soares *et al.* 2017). Upon mixing with water, the cement powder hydrates to form a poorly crystallized silicate gel (Camilleri & Pitt Ford 2006). The most intensely studied characteristics of MTA include its chemical, physical, anti-leakage and biocompatibility properties, and in this regard, MTA was reported to promote calcified barrier formation with low inflammatory response if used for root perforation repair or vital pulp therapies, respectively (Roberts *et al.* 2008, Tawil *et al.* 2015).

Currently, research interest focuses on modifying the MTA composition with the aim of improving the physical (Lee *et al.* 2011), antimicrobial (Schmalz & Galler 2017) or handling properties (Kogan *et al.* 2006). However, little attention has been paid so far to the biocompatibility testing of MTA supplied with additives (Karygianni *et al.* 2016), which furthermore have not been selected according to their cell- or tissue-supporting capabilities. Such additives would ideally (*i*) foster bone and/or pulp cell proliferation and differentiation, and hence increase hard tissue formation, while simultaneously (*ii*) being non-toxic and legally approved as a drug, and (*iii*) exerting antimicrobial actions. All of these requests are

met by fluoride (Everett 2011, Lee *et al.* 2017), thus rendering it an attractive candidate for the development of a new MTA cement (Gandolfi & Prati 2010, Gandolfi *et al.* 2011). Fluoride is reported to enhance bone mass and increase the stability of calcified tissues *in vivo*, while encouraging proliferation and osteogenic differentiation in a dose-dependent manner at the cellular level (Everett 2011). Since adequate hard tissue formation is the most challenging issue in endodontics, it is appealing to assess whether the enrichment of MTA with fluoride enhances the performance of hard tissue-forming bone cells. Hence, the aim of this study was to test the behaviour of primary human osteoblasts derived from the alveolar bone in response to fluoride-enriched MTA. The null hypothesis was that fluoride addition to MTA improves the adhesion, proliferation and differentiation of alveolar osteoblasts in terms of gene expression, matrix mineralization and alkaline phosphatase activity.

Material and Methods

MTA disk and eluate production

White Pro Root MTA powder (0.1g each; Dentsply, Konstanz, Germany) was mixed with sterile H_2O (35µl) enriched with 0.5%, 0.25%, 0.1%, which was previously checked to release 7.5×10^{-5}M , 1.7×10^{-5}M or 0.9×10^{-5}M fluoride (Merck, Darmstadt, Germany), respectively (data not shown); cement pellets without sodium fluoride addition served as controls. The cement mixtures were transferred into inverted plastic lids of Eppendorf microtubes and allowed to set for 24 h in a humidified atmosphere. The solid cement disks (0.5 cm^2 surface area, height 1.5 mm) were rinsed with 70% ethanol, washed with phosphate-buffered saline (Life Technologies, Darmstadt, Germany) and exposed to UV light under the Laminar Flow. For eluate preparation according to ISO 10993-5, MTA disks were placed for 72h in 1mL serum-free growth medium each supplemented with 1% glutamine (both Life Technologies GmbH) and 0.2% kanamycin (Sigma-Aldrich, Taufkirchen, Germany), and stored at -80 °C.

Cell culture

All experiments were carried out in accordance to the guidelines of the World Medical Association Declaration of Helsinki and were approved by the Committee of Ethics of the Medical Faculty of the Albert Ludwigs-University Freiburg, Germany (EK-153/15). Osteoblasts were isolated as described elsewhere (Proksch *et al.* 2015). Briefly, alveolar bone biopsies were minced and plated as explants in Dulbecco's Modified Eagle's medium (DMEM, LifeTechnologies) supplemented with 10% foetal bovine serum (Biochrom, Berlin, Germany), 1% glutamax (LifeTechnologies) and 1% antibiotics (Sigma Aldrich, Munich, Germany) until cell outgrowth, and cells were expanded by splitting up to 4-6 times. For analyses, cells were serum-deprived for 24h before incubation with MTA-eluate medium. Cell culture conditions were as follows: for SEM analysis, 1×10^4 cells/MTA disk in 96-well microtiter plates for 7d, for proliferation evaluation, 1×10^4 cells/well in 96-well microtiter plates for 1, 3, 5, and 7d, for gene expression analysis, 1×10^4 cells/cm^2 in T25 culture flasks for 7d, and for Alizarin red staining, 5×10^4 cells/well in 48-well multiwell plates for 21d.

Laser scanning microscopy

MTA disks were analysed using a confocal 3D laser scanning microscope (VK-X200K, Keyence Corp., Neu-Isenburg, Germany) at 20× magnification. Six regions of interest (0.04 mm^2 each) were analysed for each sample (n=5 per group) with tilt correction according to JIS B0601:2001 (ISO 4287:1997) using the VK analyzer software v3.5.0.0 (Keyence Corp.).

Scanning electron microscopy

The specimens were fixed in 4% formaldehyde and dehydrated in an ascending ethanol series (50%, 70%, 80%, 90% once each and twice in 100% for 1h). Afterwards, critical point drying (Critical Point Dryer CPD 030; Bal-Tec, Wallruf, Germany) was performed, and the samples

were sputter-coated with a gold palladium for 60s at 60mA (SCD 050; Bal-Tec) and scanned by a Zeiss Leo 435 VP scanning electron microscope at 10 kV (Zeiss, Oberkochen, Germany).

Proliferation assay

Newly synthesized DNA was measured by using a cell proliferation ELISA kit (Roche, Mannheim, Germany) according to manufacturer's instructions. In brief, cells were fixed with a one-step ready-to-use solution for 30 min at RT, and a peroxidase (POD)-labelled anti-BrdU antibody was added (1:100, 90 min, RT). The immune complexes were detected by adding tetramethyl-benzidine (30 min, RT), and the substrate reaction was stopped by adding 1 M H_2SO_4 (1:5) and quantified by measuring the absorbance at 450 nm (reference wavelength 690 nm).

qPCR

Gene expression was monitored using the RT^{2}Profiler PCR Array technology (Qiagen, Hilden, Germany). Total cellular RNA was purified using a guanidium–thiocyanate method (RNeasy Mini kit; Qiagen) and stored at -80 °C. The RNA integrity and quantity were verified using the Experion RNA StdSens chip microfluidic technology (Bio-Rad, Munich, Germany). After genomic DNA elimination and reverse transcription using the RT^2 PreAmp cDNA synthesis kit (Qiagen), one quarter of the resulting cDNA was pre-amplified using the RT^2 PreAmp Pathway Primer Mix (Quiagen). qPCR was performed in duplicate each in a CFX96 cycler (Bio-Rad), according to the manufacturer's instructions. Genomic DNA contamination, reverse transcription performance and purity, and qPCR efficiency were routinely checked. The amplicons' specificity was checked by melting curve examination. Data were collected with CFX96 Manager Software version 1.0 (Bio-Rad), and the respective genes of interest were normalized to a housekeeping gene pool comprising *ACTB*, *RPL0*, *B2M*, and *HPRT*.

Data were analyzed and plotted using the RT2 Profiler PCR array data analysis template (http://pcrdataanalysis.sabiosciences.com/ pcr/arrayanalysis). For discriminating MTA- and fluoride-related effects, the gene expression in the non-fluoride MTA group was compared to MTA-free controls. In addition, the gene expression in the respective fluoride groups was compared both to MTA-free controls and to the non-fluoride MTA group.

Alizarin red staining and extraction

Cells were incubated with 40 mM Alizarin red solution (Sigma Aldrich, pH 4.1) for 20 min at RT. After thorough washing, the air-dried specimens were evaluated with a SZH10 microscope (Olympus, Münster, Germany) equipped with a CCD Colour view III camera, and images were taken and analyzed using the Cell* software (both Olympus). For quantification, Alizarin red was extracted with 10 % acetic acid (30 min, RT). The solution was incubated for 10 min at 85 °C and the absorbance of the supernatant was read at 420 nm in triplicate. Data were collected and analyzed using the Magellan v6.2 software (Tecan, Crailsheim, Austria).

Statistical analysis

A repeated measures analysis was performed with a linear mixed model for each outcome of interest (BrdU incorporation, mM Alizarin red). The group effects and differences of least square means (LSM) were calculated with their 95-% confidence intervals. Several multiple comparisons of LSM in group and time combinations were performed and *p*-values were adjusted for multiple testing by the method of Dunnett, Tukey-Kramer or Scheffe, respectively. All calculations have been done using PROC MIXED/xtmixed from the statistical software SAS 9.1.2 (Cary, NC 27513, USA)/STATA 14.2.

Results

Osteoblasts adhere to MTA disks of comparable surface roughness irrespective of fluoride addition

Non-fluoride MTA had a mildly granular surface, which ~~became~~ obvious from a narrow range of profile values (Fig. 1a,b). This finding also applied for fluoride-enriched MTA, with 0.25% fluoride yielding a broader profile value range (Fig. 1a,b). This higher granularity was opposed to the trend of 0.1 and 0.5% fluoride to smoothen the surface (Fig. 1b). In consequence, vertical texture parameters significantly differed in the 0.25% group compared to the 0.5% fluoride group (S_p: p=0.034, S_v: p=0.018, S_z: p=0.006, S_a: p=0.016, S_q: p=0.015), while horizontal texture parameters were similar (Fig. 1b). Nevertheless, regardless of fluoride addition, the osteoblasts attached readily to MTA and formed a continuous cell layer at 7d (Fig. 1a). For all groups, the cells had a regular morphology with a blurred appearance of the cell borders (Fig. 1a). The cells exhibited a plane, triangular to rectangular shape while lacking extremely long and spindle-like cell extensions. Together, despite some roughness disparities, the cell adhesion and morphology were similar for all MTA groups irrespective of fluoride enrichment.

MTA decreases and fluoride restores the proliferation of bone cells

MTA-free control osteoblasts had a peak-to-valley proliferation pattern with initially low values that significantly increased at 5d (p<0.0001 both for 1d and 3d *vs*. 5d) before significantly decreasing at 7d (p<0.0001 5d *vs*. 7d) while still having twice the BrdU uptake of 3d (p=0.0199 3d *vs*. 7d, Fig. 2a). However, incubation with MTA eluates cleared the peak-to-valley proliferation pattern, and additionally decreased the overall cellular BrdU uptake. In detail, the proliferation of osteoblasts incubated with eluates from non-fluoride MTA did not increase at 5d and was close to zero at 7d (p=0.0501 1d *vs*. 7d, Fig. 2a). Of note, the

enrichment of MTA with fluoride partly restored the MTA-related reduction of the cellular proliferation rate in a dose-dependent manner. At 1d, osteoblasts incubated with eluates from 0.5% fluoride-MTA proliferated significantly more than non-fluoride MTA cells (p=0.0106, Fig. 2b). In all fluoride-enriched MTA groups, the BrdU uptake was significantly increased at 1d and 5d compared to 7d (p=0.0034 1d *vs.* 7d and p=0.0149 5d *vs.* 7d for 0.1% fluoride; p=0.0070 1d *vs.* 7d and p=0.0042 5d *vs.* 7d for 0.25% fluoride, and p=0.0094 1d *vs.* 7d and p=0.0507 5d *vs.* 7d for 0.5% fluoride, respectively, Fig. 2a). Although the 0.5% fluoride group proliferated significantly more at 7d compared to the 0.1% group (p=0.0334, Fig. 2b), the proliferation was significantly lower at 5d and 7d for all MTA groups compared to MTA-free controls (p<0.0001 each, Fig. 2b), irrespective of fluoride enrichment.

Both MTA and fluoride enrichment modulate the osteogenic mRNA transcription

Several MTA-related, fluoride-related and combined effects became obvious from the gene expression profiles of osteoblasts incubated with non-fluoride MTA compared to MTA-free cells (Fig. 3) and of the respective fluoride groups compared to both controls (Fig. 4). MTA incubation resulted in an up-regulation of *ALPL*, *BMP2*, *BMP3*, *BMPR1B*, *MMP10*, *NOG*, *SMAD1*, and a down-regulation of *COL15A1*, *FGF1*, *GDF10*, *MMP9*, *SERPINH1*, *SPP1* and *VCAM1* (Figs. 3 and 4). The addition of fluoride increased the transcription of *CTSK*, while *COMP*, *FGFR2* and *IGF1* were decreased (Figs. 3 and 4). Mutually intensifying effects became obvious for MTA and fluoride addition with regard to *AHSG*, *BGN*, *BMP7*, *FLT1*, *PHEX*, *TGFB2* and *VDR*, while the two substances contrarily affected the transcription of *CHRD*, *EGF*, *IGF2*, *SMAD4*, *SP7* and *TWIST1* (Figs. 3 and 4). Although *VEGFB* was up-regulated in cells incubated with eluates from the 0.1% (Fig. 4a) and the 0.25% fluoride-MTA group (Fig. 4b), this effect became significant only in the 0.5% fluoride group compared to

MTA-free controls (p=0218, Fig. 4c). Moreover, high-dose fluoride enrichment modulated the expression of *BGLAP*, *BGN*, *COL10A1*, *FN1*, *ICAM1*, *RUNX2*, and *VEGFA*, while further dose-related effects were visible for *ITGA2* and, again, *SPP1* (Figs. 3 and 4). *CD36* was up-regulated in all fluoride-enriched groups relative to MTA-free controls (Fig. 4a-c), while being unchanged compared to the non-fluoride MTA group (Fig. 4d-f), and if comparing the non-fluoride MTA group to MTA-free controls (Fig. 3a,b). This finding points to a combined effect of MTA and fluoride that is not noticeable for either of them alone. For the transcriptome profiling, all genes with a fold regulation change >|1.5| were taken into account for analysis, while admittedly rather expression changes >|2| are considered biologically meaningful. Nevertheless, the mRNA quantity of some genes with expression changes <|2| was modulated in a statistically significant way, while genes showing expression modulation up to |8| did not reach the mathematical significance level. Hence, expression changes of large magnitudes, as seen for *COMP*, *COL15a1*, *IGF1*, *MMP10*, *MMP9*, and *NOG*, are supposed to influence a biological system even if they appear non-significant. Together, MTA-related effects became visible mainly for mRNAs relevant for osteogenic differentiation and extracellular matrix formation, and the latter group was also mostly influenced by dose-dependent fluoride effects.

Fluoride enhances the MTA-impaired extracellular matrix mineralization

The modulation of the transcriptome profile both by MTA and fluoride led the investigation of the extracellular matrix mineralization, which is regarded as the hallmark of osteogenic differentiation and the ultimate prerequisite for hard tissue restoration. Compared to MTA-free controls (Fig. 5a), incubation with eluates from non-fluoride MTA (Fig. 5b) significantly reduced matrix calcification (p<0.0001). The same applied for osteoblasts incubated with eluates from MTA enriched with 0.1% (Fig. 5c, p<0.0001), 0.25% (Fig. 5d, p<0.0001), and 0.5% fluoride (Fig. 5e, p<0.0001, Fig. 5f). However, the addition of fluoride essentially

supported matrix mineralization in a dose-dependent manner. Similar to the non-fluoride MTA group, the 0.1% fluoride-MTA group was not associated with noteworthy calcium deposits. However, osteoblasts incubated with 0.25% fluoride-MTA had significantly more Alizarin red staining compared both to non-fluoride MTA (p=0.0022, Fig. 5f) and compared to 0.1% fluoride-MTA (p=0.0058, Fig. 5f). The amount of dye was even increased in the 0.5% fluoride group (p=0.0006 vs. non-fluoride MTA and p=0.0017 vs. 0.1% fluoride-MTA, Fig. 5f).

Discussion

Mineral trioxide aggregate is considered the gold standard therapeutic agent for hard tissue induction purposes (Karygianni *et al.* 2016, Lv *et al.* 2017). The results of the present study reveal that the enrichment of ProRoot MTA with fluoride improves its biocompatibility in terms of osteoblast proliferation, osteogenic gene expression and extracellular matrix mineralization, while the cement texture modifies neither the cell adhesion nor morphology.

Basically, tissue cells react to their environment, i.e. the presence of fluoride-enriched ProRoot MTA, by (*i*) focal adhesion-mediated processing of biomechanical signals and (*ii*) perception of eluted biomolecules (Engler *et al.* 2009). For biomechanical sensing, osteoblasts seize the elasticity and topology of MTA by anchoring to the cement *via* focal adhesion sites (Giancotti & Ruoslahti 1999, Fletcher & Mullins 2010), which facilitate the reciprocal transformation of biomechanical to biochemical signals (Tomakidi *et al.* 2014). Generally, the physical properties of solidified MTA largely rely on handling parameters such as powder/liquid ratio (Basturk *et al.* 2015), mixing method (Nekoofar *et al.* 2010, Basturk *et al.* 2014, Duque *et al.* 2018), condensation pressure (Nekoofar *et al.* 2007), environmental humidity (Caronna *et al.* 2014, Shokouhinejad *et al.* 2014) and pH (Bolhari *et al.* 2014), all being constant in ~~the~~ experimental setup. From a chemical viewpoint, mixing the MTA

powder with fluoride-enriched water is assumed to result in chemical integration of fluoride into the solidifying crystal structures (Song *et al.* 2006, Parirokh & Torabinejad 2010), which probably sustains physical characteristics similar to non-fluoride ProRoot MTA (Appelbaum *et al.* 2012). Hence, the elasticity of fluoride-enriched MTA is supposed to be in the range of non-fluoride MTA (Haecker *et al.* 2005). Since the order of magnitude manipulating cellular lineage specification (Engler *et al.* 2006) is far below, the changes resulting from fluoride addition to MTA might be irrelevant for bone cells. Regarding topographical cues, it can be speculated that 0.25% fluoride modulates the size of MTA crystals during the hydration process (Camilleri 2007). Nevertheless, regardless of any roughness disparities, the adherent bone cells were similar in shape and number. Although it cannot be ruled out that topological cues may affect bone cell behavior (Iskratsch *et al.* 2014), this finding suggests that investigating the cellular responses to biochemical signals as a function of fluoride enrichment appears more compelling in the first place. As a consequence, it was decided to focus on the analysis of eluate-related, i.e. biochemically induced rather than adhesion-related effects of MTA with and without fluoride addition.

In fact, two main points became obvious from eluate testing: first, ProRoot MTA itself decreased proliferation and extracellular matrix formation of alveolar osteoblasts, and scores of genes involved in osteogenesis, bone mineral metabolism and extracellular matrix formation were modulated. Second, the addition of fluoride supported the bone cell proliferation and matrix calcification, and modulated the transcription of *COMP*, *CTSK*, *IGF1* and *FGFR2* independently from MTA-related effects, while further genes were regulated in a dose-dependent manner in response to the ProRoot MTA presence. The finding that ProRoot MTA delayed both bone cell proliferation and differentiation seems surprising because it is widely accepted that MTA is highly biocompatible (Camilleri & Pitt Ford 2006, Lv *et al.* 2017) and supports hard tissue formation (Parirokh & Torabinejad 2010, Katsamakis *et al.* 2013). However, the term ‘biocompatibility’ in general refers to the degree of a material’s

toxicity, which is usually measured by means of phenotyping, monitoring the inflammatory response or the metabolic activity of target cells, while behavioral parameters such as cell division or differentiation are not addressed. Actually, a number of reports show that cellular proliferation and differentiation are diminished by MTA if compared to native controls (Nakayama *et al.* 2005, Hakki *et al.* 2009, Willershausen *et al.* 2013, Suzuki *et al.* 2015); and it is not surprising that cells in contact with any repair material perform worse compared to untouched controls. A subtle but important difference is that MTA indeed supports the cellular performance if compared to other endodontic materials (Nakayama *et al.* 2005), which were not investigated in the framework of this study. Hence, the present data do not conflict with MTA being biocompatible and tissue-supportive.

Fluoride improved the MTA-altered cell behavior by proliferation enhancement and differentiation boosting of alveolar osteoblasts, thereby confirming current knowledge on the action of sodium fluoride on bone cells (Everett 2011, Lee *et al.* 2017). Of note, the effects seen in the present study originate from fluoride that was eluted from MTA disks, which means that fluoride-enriched MTA does release bioactive fluoride. Although the wash-out fluoride concentration was not determined, the responses of osteoblasts unequivocally show that mitogenic and differentiation-inducing levels were present. With regard to the transcriptome, a peculiar finding was that fluoride affected the transcription of *COMP*, which is usually associated with enchondral ossification in long bones (Di Cesare *et al.* 2000) while being rarely described in alveolar osteoblasts. Obviously in the present study, the vast majority of genes modulated by MTA are related to osteogenic differentiation and extracellular matrix formation, while the effects of fluoride also covered the field of intercellular communication, growth factor and cytokine genes in skeletal development. This screening for transcriptional changes profoundly contributes to the understanding of the mechanisms of both MTA and fluoride actions on osteoblasts by disclosing single and combined effects of both substances. In addition to such cellular effects, fluoride

physicochemically interacts with bone mineral matrix by conversion of hydroxyapatite to fluorapatite (Everett 2011). Since both compounds contain equimolecular amounts of calcium, the intensified matrix mineralization presumably results from a real stimulation of osteogenic differentiation. This interpretation is emphasized by the finding that high-dose fluoride mainly affects the transcription of genes encoding for extracellular matrix proteins, reflecting the dose-related increase in matrix calcification. In clinical situations, local fluoride release has already been shown to enhance osteoblastic differentiation and bone formation (Cooper *et al.* 2006, Monjo *et al.* 2008); hence it can be speculated that similar effects are found for MTA containing fluoride *in vivo*.

Conclusion

The addition of sodium fluoride to ProRoot MTA cement supports the proliferation and differentiation of alveolar osteoblasts. Thus, fluoride enrichment opens up new horizons for the development of new MTA-based therapies that promote hard tissue formation in endodontics.

References

Appelbaum KS, Stewart JT, Hartwell GR (2012) Effect of sodium fluorosilicate on the properties of Portland cement. *Journal of Endodontics* **38,** 1001-3.

Basturk FB, Nekoofar MH, Gunday M, Dummer PM (2014) Effect of various mixing and placement techniques on the flexural strength and porosity of mineral trioxide aggregate. *Journal of Endodontics* **40,** 441-5.

Basturk FB, Nekoofar MH, Gunday M, Dummer PM (2015) Effect of varying water-to-powder ratios and ultrasonic placement on the compressive strength of mineral trioxide aggregate. *Journal of Endodontics* **41,** 531-4.

Bolhari B, Nekoofar MH, Sharifian M, Ghabrai S, Meraji N, Dummer PM (2014) Acid and microhardness of mineral trioxide aggregate and mineral trioxide aggregate-like materials. *Journal of Endodontics* **40,** 432-5.

Camilleri J (2007) Hydration mechanisms of mineral trioxide aggregate. *International Endodontic Journal* **40,** 462-70.

Camilleri J, Pitt Ford TR (2006) Mineral trioxide aggregate: a review of the constituents and biological properties of the material. *International Endodontic Journal* **39,** 747-54.

Caronna V, Himel V, Yu Q, Zhang JF, Sabey K (2014) Comparison of the surface hardness among 3 materials used in an experimental apexification model under moist and dry environments. *Journal of Endodontics* **40,** 986-9.

Cooper LF, Zhou Y, Takebe J *et al.* (2006) Fluoride modification effects on osteoblast behavior and bone formation at TiO2 grit-blasted c.p. titanium endosseous implants. *Biomaterials* **27,** 926-36.

Di Cesare PE, Fang C, Leslie MP, Tulli H, Perris R, Carlson CS (2000) Expression of cartilage oligomeric matrix protein (COMP) by embryonic and adult osteoblasts. *Journal of Orthopaedic Research* **18,** 713-20.

Duque JA, Fernandes SL, Bubola JP, Duarte MAH (2018) The effect of mixing method on tricalcium silicate-based cement. *International Endodontic Journal* **51,** 69-78.

Engler AJ, Humbert PO, Wehrle-Haller B, Weaver VM (2009) Multiscale modeling of form and function. *Science* **324,** 208-12.

Engler AJ, Sen S, Sweeney HL, Discher DE (2006) Matrix elasticity directs stem cell lineage specification. *Cell* **126,** 677-89.

Everett ET (2011) Fluoride's effects on the formation of teeth and bones, and the influence of genetics. *Journal of Dental Research* **90,** 552-60.

Fletcher DA, Mullins RD (2010) Cell mechanics and the cytoskeleton. *Nature* **463,** 485-92.

Gandolfi MG, Prati C (2010) MTA and F-doped MTA cements used as sealers with warm gutta-percha. Long-term study of sealing ability. *International Endodontic Journal* **43,** 889-901.

Gandolfi MG, Taddei P, Siboni F, Modena E, Ginebra MP, Prati C (2011) Fluoride-containing nanoporous calcium-silicate MTA cements for endodontics and oral

surgery: early fluorapatite formation in a phosphate-containing solution. *International Endodontic Journal* **44,** 938-49.

Giancotti FG, Ruoslahti E (1999) Integrin signaling. *Science* **285,** 1028-32.

Grazziotin-Soares R, Nekoofar MH, Davies T, Hubler R, Meraji N, Dummer PMH (2017) Crystalline phases involved in the hydration of calcium silicate-based cements: Semi-quantitative Rietveld X-ray diffraction analysis. *Australian Endodontic Journal* [doi: 10.1111/aej.12226]

Haecker C-J, Garboczi EJ, Bullard JW *et al.* (2005) Modeling the linear elastic properties of Portland cement paste. *Cement and Concrete Research* **35,** 1948-60.

Hakki SS, Bozkurt SB, Hakki EE, Belli S (2009) Effects of mineral trioxide aggregate on cell survival, gene expression associated with mineralized tissues, and biomineralization of cementoblasts. *Journal of Endodontics* **35,** 513-9.

Iskratsch T, Wolfenson H, Sheetz MP (2014) Appreciating force and shape-the rise of mechanotransduction in cell biology. *Nature Reviews Molecular Cell Biology* **15,** 825-33.

Karygianni L, Proksch S, Schneider S *et al.* (2016) The effects of various mixing solutions on the biocompatibility of mineral trioxide aggregate. *International Endodontic Journal* **49,** 561-73.

Katsamakis S, Slot DE, Van der Sluis LW, Van der Weijden F (2013) Histological responses of the periodontium to MTA: a systematic review. *Journal of Clinical Periodontology* **40,** 334-44.

Kogan P, He J, Glickman GN, Watanabe I (2006) The effects of various additives on setting properties of MTA. *Journal of Endodontics* **32,** 569-72.

Lee BN, Hwang YC, Jang JH *et al.* (2011) Improvement of the properties of mineral trioxide aggregate by mixing with hydration accelerators. *Journal of Endodontics* **37,** 1433-6.

Lee M, Arikawa K, Nagahama F (2017) Micromolar Levels of Sodium Fluoride Promote Osteoblast Differentiation Through Runx2 Signaling. *Biological Trace Element Research* **178,** 283-91.

Lee YL, Lee BS, Lin FH, Yun Lin A, Lan WH, Lin CP (2004) Effects of physiological environments on the hydration behavior of mineral trioxide aggregate. *Biomaterials* **25,** 787-93.

Lv F, Zhu L, Zhang J, Yu J, Cheng X, Peng B (2017) Evaluation of the in vitro biocompatibility of a new fast-setting ready-to-use root filling and repair material. *International Endodontic Journal* **50,** 540-48.

Monjo M, Lamolle SF, Lyngstadaas SP, Ronold HJ, Ellingsen JE (2008) In vivo expression of osteogenic markers and bone mineral density at the surface of fluoride-modified titanium implants. *Biomaterials* **29,** 3771-80.

Nakayama A, Ogiso B, Tanabe N, Takeichi O, Matsuzaka K, Inoue T (2005) Behaviour of bone marrow osteoblast-like cells on mineral trioxide aggregate: morphology and expression of type I collagen and bone-related protein mRNAs. *International Endodontic Journal* **38,** 203-10.

Nekoofar MH, Adusei G, Sheykhrezae MS, Hayes SJ, Bryant ST, Dummer PM (2007) The effect of condensation pressure on selected physical properties of mineral trioxide aggregate. *International Endodontic Journal* **40,** 453-61.

Nekoofar MH, Aseeley Z, Dummer PM (2010) The effect of various mixing techniques on the surface microhardness of mineral trioxide aggregate. *International Endodontic Journal* **43,** 312-20.

Nekoofar MH, Davies TE, Stone D, Basturk FB, Dummer PM (2011) Microstructure and chemical analysis of blood-contaminated mineral trioxide aggregate. *International Endodontic Journal* **44,** 1011-8.

Parirokh M, Torabinejad M (2010) Mineral trioxide aggregate: a comprehensive literature review--Part I: chemical, physical, and antibacterial properties. *Journal of Endodontics* **36,** 16-27.

Parirokh M, Torabinejad M (2010) Mineral trioxide aggregate: a comprehensive literature review--Part III: Clinical applications, drawbacks, and mechanism of action. *Journal of Endodontics* **36,** 400-13.

Proksch S, Bittermann G, Vach K, Nitschke R, Tomakidi P, Hellwig E (2015) hMSC-Derived VEGF Release Triggers the Chemoattraction of Alveolar Osteoblasts. *Stem Cells* **33,** 3114-24.

Roberts HW, Toth JM, Berzins DW, Charlton DG (2008) Mineral trioxide aggregate material use in endodontic treatment: a review of the literature. *Dental Materials* **24,** 149-64.

Schmalz G, Galler KM (2017) Biocompatibility of biomaterials - Lessons learned and considerations for the design of novel materials. *Dental Materials* **33,** 382-93.

Shokouhinejad N, Jafargholizadeh L, Khoshkhounejad M, Nekoofar MH, Raoof M (2014) Surface microhardness of three thicknesses of mineral trioxide aggregate in different setting conditions. *Restorative Dentistry & Endodontics* **39,** 253-7.

Song JS, Mante FK, Romanow WJ, Kim S (2006) Chemical analysis of powder and set forms of Portland cement, gray ProRoot MTA, white ProRoot MTA, and gray MTA-Angelus. *Oral Surgery, Oral Medicine, Oral Pathology, Oral Radiology, and Endodontics* **102,** 809-15.

Suzuki Y, Hayashi M, Tanabe N *et al.* (2015) Effect of a novel fluorapatite-forming calcium phosphate cement with calcium silicate on osteoblasts in comparison with mineral trioxide aggregate. *Journal of Oral Sciences* **57,** 25-30.

Tawil PZ, Duggan DJ, Galicia JC (2015) Mineral trioxide aggregate (MTA): its history, composition, and clinical applications. *Compendium of Continuing Education in Dentistry* **36,** 247-52.

Tomakidi P, Schulz S, Proksch S, Weber W, Steinberg T (2014) Focal adhesion kinase (FAK) perspectives in mechanobiology: implications for cell behaviour. *Cell Tissue Research* **357,** 515-26.

Willershausen I, Wolf T, Kasaj A, Weyer V, Willershausen B, Marroquin BB (2013) Influence of a bioceramic root end material and mineral trioxide aggregates on fibroblasts and osteoblasts. *Archives of Oral Biology* **58,** 1232-7.

Figure Captions

Figure 1: Representative images (a) and surface roughness values (b) of non-fluoride MTA and fluoride-enriched MTA, respectively. (**a**) Laser scanning images, 3D surface roughness views and scanning electron microscopy images of MTA disks without fluoride (top row, H_2O) or with the addition of 0.1% (second row), 0.25% (third row), or 0.5% fluoride (lower row) without (LSM and 3D views) and with alveolar osteoblasts, respectively. (**b**) S_p: maximum profile peak height, S_v: maximum profile valley depth, S_z: maximum height of profile, S_a: arithmetic mean height, S_q: root mean square height, S_{sk}: skewness, S_{ku}: kurtosis. Data are presented as mean±SD values.

Figure 2: Bar graph diagrams showing the proliferation of osteoblasts undergoing incubation with eluates from non-fluoride MTA (H_2O, black bars) and from fluoride-enriched MTA (0.1, 0.25, 0.5, respectively, shaded bars) compared to MTA-free controls (w/o, white bars) at 1, 3, 5, and 7 d. (**a**) Time-dependent proliferation change within the different groups and (**b**) inter-group comparison at different time points.

Figure 3: Osteogenic marker gene transcription (a) in osteoblasts incubated with eluates from non-fluoride MTA relative to MTA-free controls and (b) in all groups. (**a**) Volcano plots of qPCR data display statistical significance (y-axis) versus fold change (x-axis), respectively, with 1.5 as fold-change cutoff (vertical black lines) and $p<0.05$ (horizontal green line). Blue: down-regulated genes, grey: non-regulated genes, red: up-regulated genes. (**b**) Selection of genes which are modulated either by MTA or fluoride alone, or by a combination of both, respectively (see text for details). Fold regulation changes >2 are depicted in bold letters, and statistically significant changes are labeled with (*).

Figure 4: Compilation of qPCR data volcano plots of osteoblasts incubated with fluoride-enriched MTA eluates relative to MTA-free controls (vs. w/o, a-c) and to cells incubated with non-fluoride MTA eluates (vs. H_2O, d-e). The comparison of (a) with (d), (b) with (e) and (c) with (f) reveals fluoride-dependent changes is gene expression.

Figure 5: Representative images of Alizarin red stains of MTA-free cells (a), and osteoblasts incubated with eluates from non-fluoride MTA (b), or MTA enriched with 0.1% (c), 0.25% (d), or 0.5% fluoride (e), respectively, after 21 d in culture without addition of further mineralization-inducing agents. (f) Box plot diagram of extracted Alizarin red dye of osteoblasts incubated with MTA eluates compared to MTA-free controls (w/o).

(a)

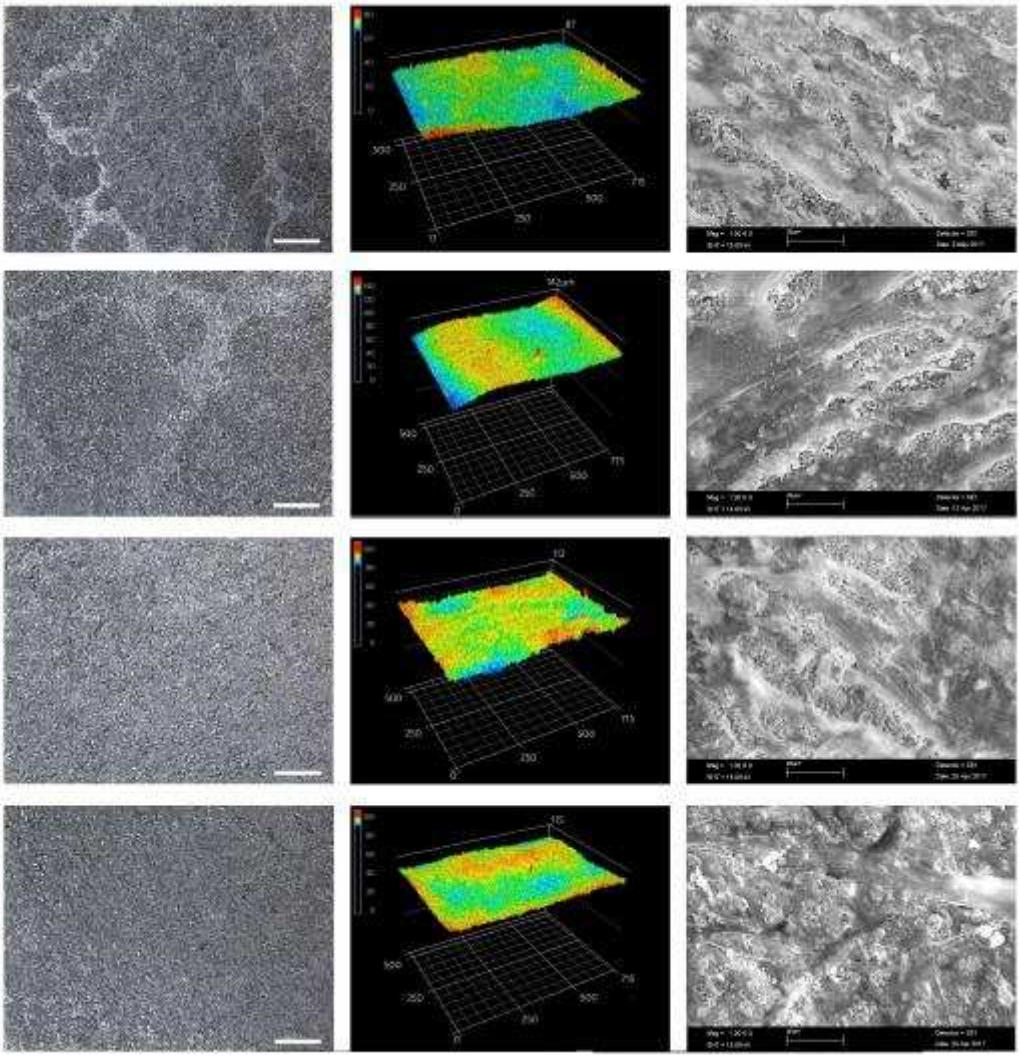

(b)

	H_2O	0.1%	0.25%	0.5%
S_p	14.21±3.99	12.88±5.51	14.01±5.75	9.49±2.99
S_v	10.80±3.72	9.66±3.44	14.65±10.45	7.08±1.06
S_z	25.01±7.19	22.54±7.69	28.67±12.72	16.57±3.09
S_a	2.46±1.25	2.13±0.91	2.99±1.53	1.38±0.26
S_q	3.12±1.51	2.71±1.12	3.73±1.83	1.75±0.28
S_{sk}	0.32±0.41	0.29±0.56	0.00±0.59	0.15±0.34
S_{ku}	3.67±0.86	4.08±1.70	3.53±1.58	3.83±1.34

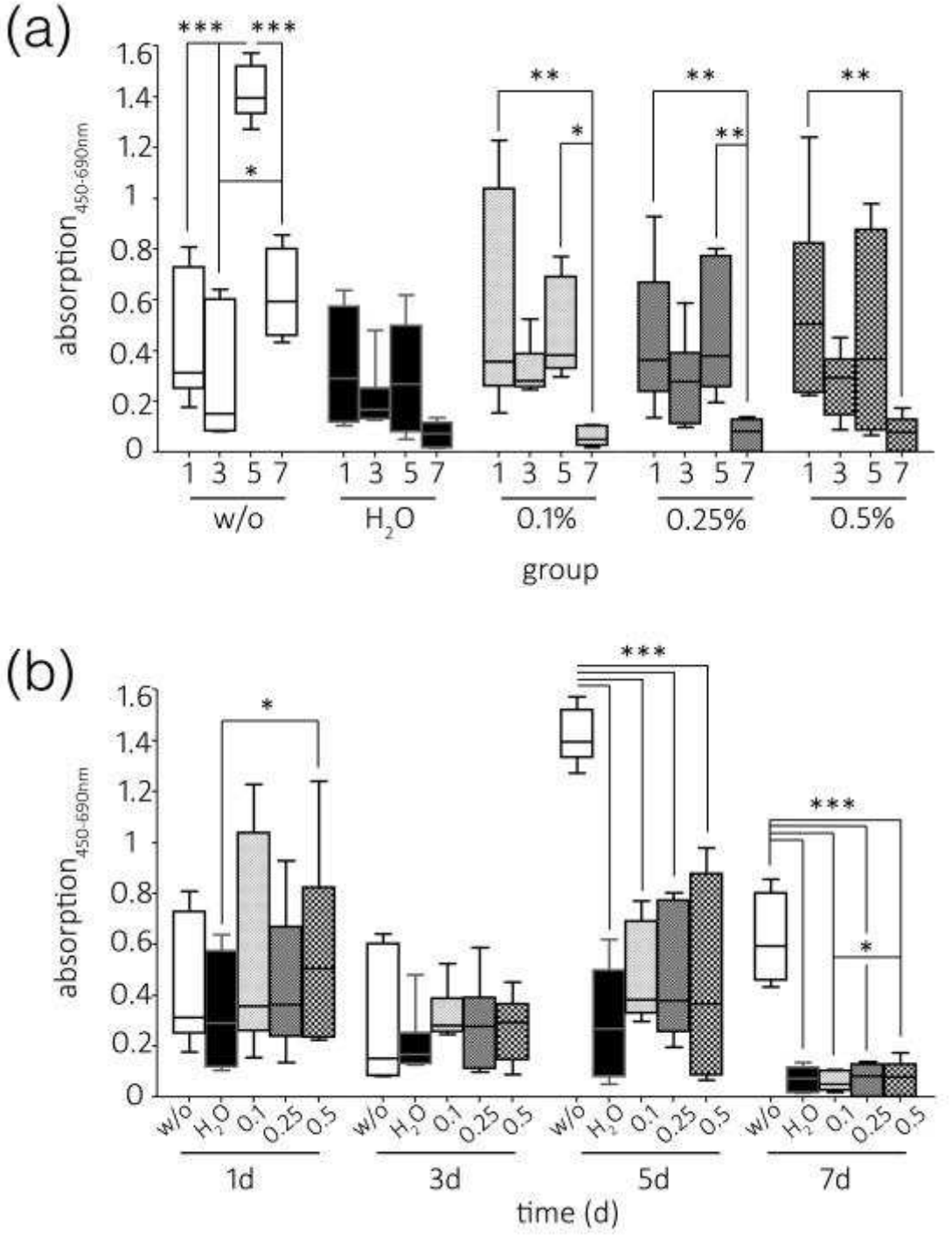
(a)
absorption450-690nm
1.6
1.4
1.2
1
0.8
0.6
0.4
0.2
0
***
***
*
**
*
**
**
**
1 3 5 7
w/o
H2O
0.1%
0.25%
0.5%
group
(b)
absorption450-690nm
*
***
***
*
w/o
H2O
0.1
0.25
0.5
1d
3d
5d
7d
time (d)

(a)

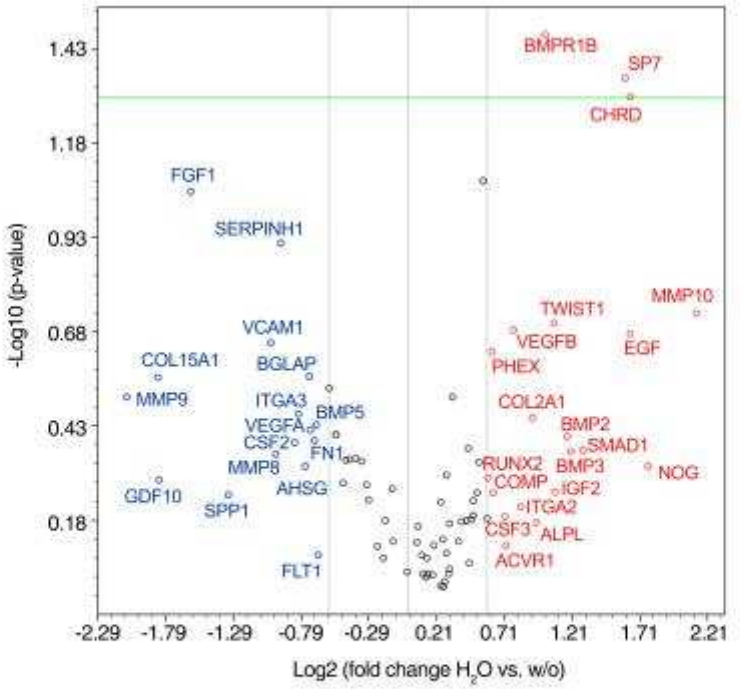

(b)

		Up-down regulation compared to w/o				Up-down regulation compared to H_2O		
	gene	0.1%	0.25%	0.5%	H_2O	0.1%	0.25%	0.5%
osteoblast differentiation and osteogenesis	AHSG	-1.9914	**-2.3849**	**-2.5342**	-1.6882	-1.1796	-1.4127	-1.5011
	ALPL	1.6267	1.4230	1.8030	1.9330	-1.1883	-1.3584	-1.0721
	BMP2	**2.7537**	**3.4983**	**2.9673**	**2.2579**	1.2240	1.5494	1.3142
	BMP3	**2.3445**	1.9901	1.6070	**2.2987**	1.0199	-1.1551	-1.4304
	BMP7	-1.8206	1.0807	**-2.0075**	-1.3464	-1.3522	1.4551	-1.4910
	BMPR1B	**2.0564**	1.9703	*1.8502	***2.0171**	1.0196	-1.0238	-1.0902
	CHRD	1.3920	1.8656	1.1398	***3.1205**	**-2.2417**	-1.6727	**-2.7377**
	COMP	**-4.1874**	**-2.7500**	**-5.1996**	1.5467	**-6.4766**	**-4.2534**	**-8.0423**
	DLX5	1.1241	-1.6152	-1.1277	1.3976	-1.2433	**-2.2575**	-1.5761
	GDF10	**-2.8929**	**-4.5686**	**-3.0476**	**-3.5632**	1.2317	-1.2821	1.1692
	NOG	**4.4789**	**3.8925**	**2.1353**	**3.4219**	1.3089	1.1375	-1.6025
	SMAD1	**2.1028**	1.9625	1.9194	**2.4515**	-1.1658	-1.2491	-1.2772
	SMAD4	1.1982	1.1693	1.1020	1.4651	*-1.2236	*-1.2538	*-1.3303
	SP7	1.7845	1.7609	1.8719	***3.0418**	-1.7046	-1.7275	-1.6250
	TWIST1	1.4961	1.4948	1.4840	**2.1126**	-1.4121	-1.4133	-1.4236
cytokines and receptors in skeletal development	EGF	1.6063	**2.0653**	1.4664	**3.1141**	-1.9387	-1.5078	**-2.1236**
	FGF1	-1.9105	**-2.2170**	**-2.0495**	**-3.0314**	1.5867	1.3673	1.4791
	FGFR2	**-2.0801**	**-2.1135**	**-3.7060**	-1.3749	-1.5129	-1.5372	**-2.6954**
	FLT1	**-2.1516**	**-2.6212**	**-2.2875**	-1.5803	-1.3615	-1.6586	-1.4475
	ICAM1	1.4247	1.4939	**2.1183**	1.1941	1.1931	1.2510	1.7739
	IGF1	**-3.8413**	**-2.1819**	**-4.1346**	1.4962	**-5.7475**	**-3.2646**	**-6.1864**
	IGF2	1.3290	-1.5418	-1.8073	**2.1201**	-1.5953	**-3.2688**	**-3.8316**
	TGFB2	**-2.1505**	**-2.1444**	**-2.3345**	-1.4991	-1.4346	-1.4305	-1.5573
	TGFBR1	-1.6568	-1.2261	-1.3503	1.0610	-1.7909	-1.3255	-1.4597
	VDR	-1.3419	-1.1139	-1.5458	1.1399	-1.5297	-1.2697	-1.7621
	VEGFA	-1.3178	-17291	-2.5352	-1.6455	1.2487	-1.0508	-1.5406
	VEGFB	1.7684	1.7563	***2.2911**	1.7188	1.0289	1.0218	1.3330
extracellular matrix formation and remodelling	BGLAP	-1.3156	-1.5719	**-2.2268**	-1.6576	1.2600	1.0545	-1.3434
	BGN	-1.7239	-1.8136	**-2.4143**	-1.3044	-1.3216	-1.3903	*-1.8509
	CD36	1.7667	1.9150	1.6558	1.3815	1.2789	1.3862	1.1986
	CTSK	***2.7188**	***3.0062**	***4.2058**	1.1835	**2.2973**	**2.5401**	***3.5537**
	COL10A1	1.1013	-1.3778	-1.6731	1.1831	-1.0743	-1.6301	*-1.9794
	COL15A1	**-2.7966**	**-4.0868**	**-4.0926**	**-3.5882**	1.2931	-1.1390	-1.1406
	FN1	-1.4987	-1.6362	-1.9657	-1.6140	1.0770	-1.0137	-1.2179
	ITGA2	1.7881	1.4594	-1.3184	1.7826	1.0031	-1.2215	**-2.3501**
	MMP8	-1.2264	**-3.4808**	**-3.0451**	-1.9631	1.6007	-1.7732	-1.5512
	MMP9	**-5.9047**	**-4.8628**	**-4.7702**	**-4.2226**	-1.3983	-1.1516	-1.1297
	MMP10	**6.4135**	**4.7851**	**2.4930**	**4.3775**	1.4651	1.0931	-1.7559
	PHEX	**2.4140**	**2.1463**	***2.0472**	1.5398	1.5678	1.3939	1.3295
	RUNX2	1.1464	1.1704	-1.2266	1.5045	-1.3123	-1.2854	*-1.8453
	SERPINH1	-1.8727	**-2.1902**	**-2.0534**	-1.9223	1.0265	-1.1393	-1.0682
	SPP1	**2.0580**	1.0984	**-2.7715**	**-2.5129**	**5.1715**	**2.7602**	-1.1029
	VCAM1	-1.8383	**-2.4335**	**-2.4788**	**-2.0202**	1.0991	-1.2044	-1.2268

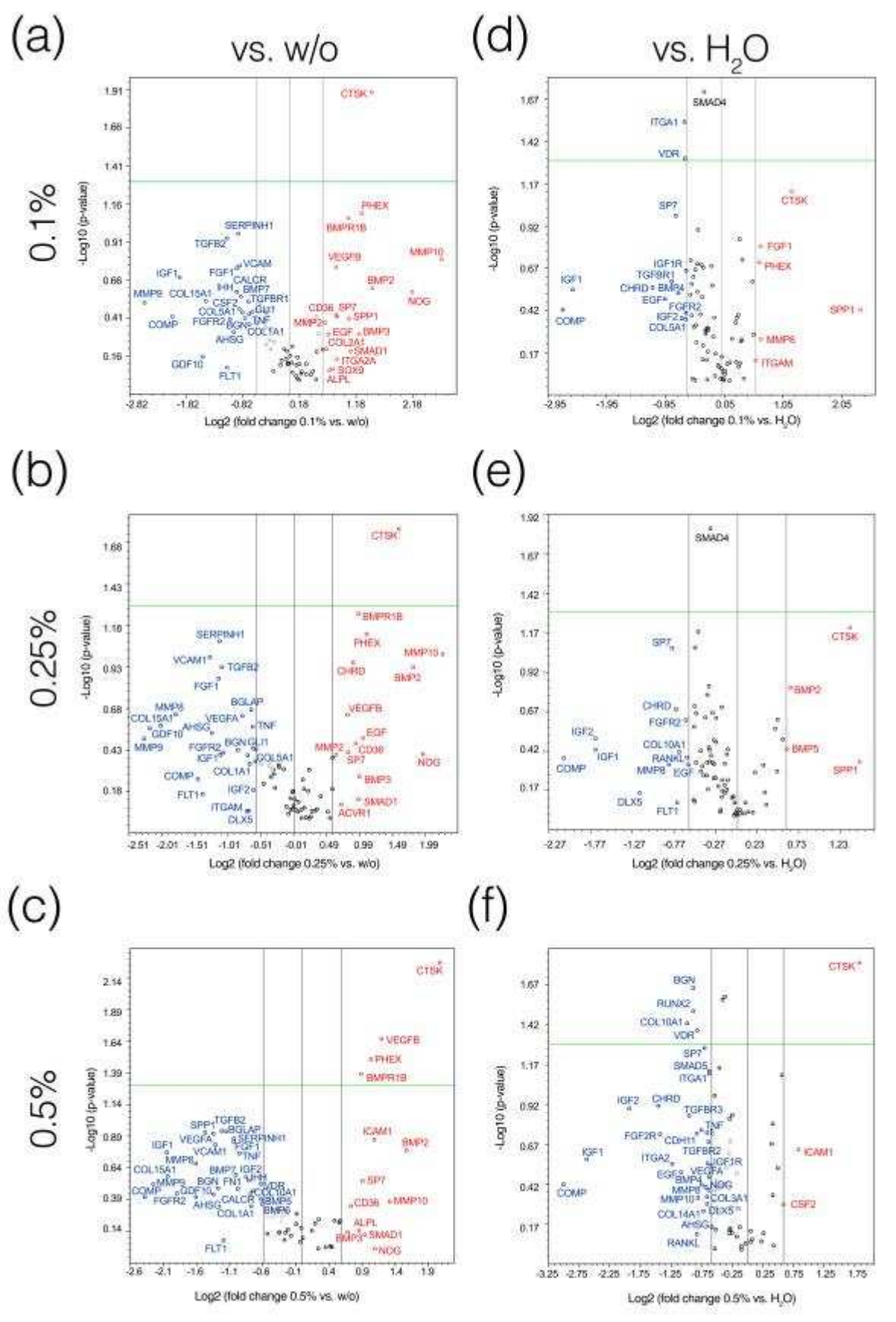
(a)
vs. w/o
(d)
vs. H2O
0.1%
-Log10 (p-value)
Log2 (fold change 0.1% vs. w/o)
Log2 (fold change 0.1% vs. H2O)
(b)
(e)
0.25%
Log2 (fold change 0.25% vs. w/o)
Log2 (fold change 0.25% vs. H2O)
(c)
(f)
0.5%
Log2 (fold change 0.5% vs. w/o)
Log2 (fold change 0.5% vs. H2O)

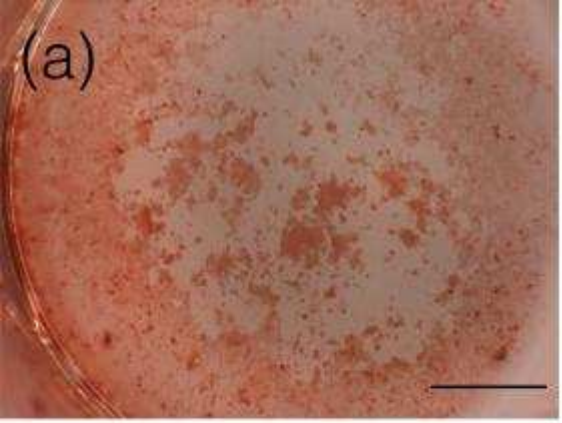
(a)

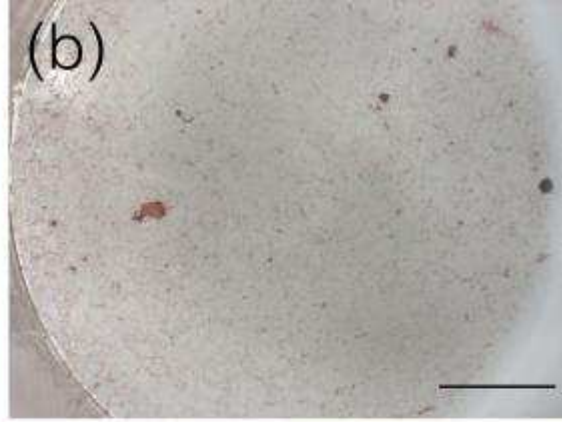
(b)

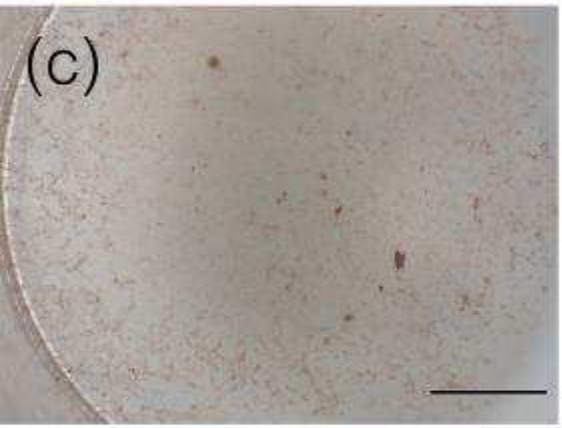
(c)

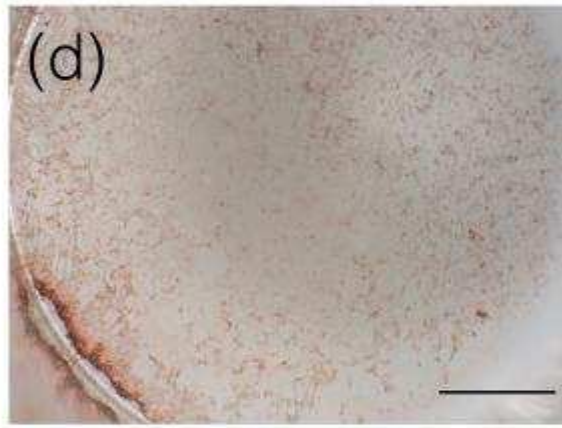
(d)

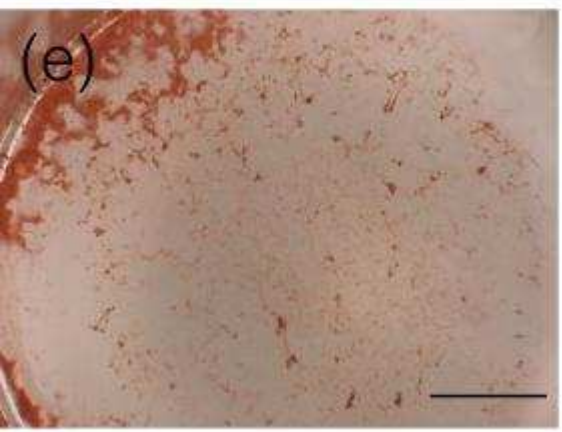
(e)

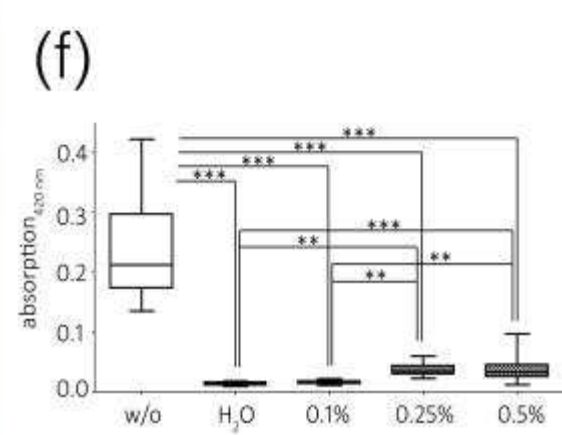
(f)
absorption 420 nm
0.4
0.3
0.2
0.1
0.0
***
***
***
***
***
**
**
**
w/o
H2O
0.1%
0.25%
0.5%